The synthesis and *in vitro* testing of a zinc-activated MRI contrast agent

Jody L. Major*, Giacomo Parigi†, Claudio Luchinat†, and Thomas J. Meade*‡§¶‖

Departments of *Chemistry, ‡Biochemistry and Molecular and Cell Biology, §Neurobiology and Physiology, and ¶Radiology, Northwestern University, 2145 Sheridan Road, Evanston, IL 60208; and †Magnetic Resonance Center (CERM), Fiorgen Pharmacogenomic Foundation, and Department of Agricultural Biotechnology, University of Florence, Via Luigi Sacconi, 6, 50019 Florence, Italy

Communicated by Brian M. Hoffman, Northwestern University, Evanston, IL, July 3, 2007 (received for review May 20, 2007)

Zinc(II) plays a vital role in normal cellular function as an essential component of numerous enzymes, transcription factors, and synaptic vesicles. While zinc can be linked to a variety of physiological processes, the mechanisms of its cellular actions are less discernible. Here, we have synthesized and tested a Zn(II)-activated magnetic resonance imaging (MRI) contrast agent in which the coordination geometry of the complex rearranges upon binding of Zn(II). In the absence of Zn(II) water is restricted from binding to a chelated Gd(III) ion by coordinating acetate arms resulting in a low relaxivity of 2.33 $mM^{-1}\cdot s^{-1}$ at 60 MHz. Upon addition of Zn(II) the relaxivity of the Gd(III)–Zn(II) complex increases to 5.07 $mM^{-1}\cdot s^{-1}$ and is consistent with one water molecule bound to Gd(III). These results were confirmed by nuclear magnetic relaxation dispersion analysis. There was no observed change in relaxivity of the Gd(III) complex when physiologically competing cations Ca(II) and Mg(II) were added. A competitive binding assay gave a dissociation constant of 2.38 × 10^{-4} M for the Gd(III)–Zn(II) complex. *In vitro* magnetic resonance images confirm that Zn(II) concentrations as low as 100 μM can be detected by using this contrast agent.

biological molecular imaging | zinc sensing | gadolinium

Zinc(II) plays a critical role in cellular physiology and is involved in structural stability, catalytic activity, and signal transduction processes (1–3). While a great deal is known about the biochemistry of Zn(II) in relation to metalloproteins, far less is understood about the specific mechanisms of its cellular physiology and distribution because it is tightly bound to zinc-binding ligands (4). To understand the specific functions of Zn(II), research has focused on the development of Zn(II) fluorescent probes (5, 6). These Zn(II) probes are changing our understanding of the biological function of this important ion in cell and tissue culture experiments.

Our goal has been to noninvasively image Zn(II) activity in whole organisms, and we have focused on developing Zn(II) magnetic resonance (MR) contrast agents. Unlike light-based microscopy, MRI can provide three-dimensional images without the limitations of light scattering and photobleaching (7, 8). MRI takes advantage of the most abundant molecule in biological tissues, water. In the presence of a magnetic field the magnetic moments of the protons in water molecules orient themselves along the magnetic field. An applied radiofrequency pulse inverts the magnetization vector, and reorientation to the original magnetic field direction occurs with a characteristic time constant. This process of realignment characterized by T_1 is called longitudinal or spin-lattice relaxation, and it is the dominant factor in producing contrast in a T_1-weighted MR image. While intrinsic contrast between organs can be observed by using MRI, resolution and sensitivity improve greatly with the use of contrast agents such as Gd(III) chelates. The efficacy of these complexes to decrease the T_1 of the local water protons, and therefore brighten the image, is measured by their relaxivity values ($mM^{-1}\cdot s^{-1}$) (7, 8).

Recently, a new class of biologically activated MR contrast agents has been developed in which a change in the relaxivity of the agent is observed during binding of cations, changes in pH, and enzyme activity (9–12). Three variables dominate an observed change in T_1 of a contrast agent: the rotational correlation time (τ_R), the exchange correlation time (τ_m), and the number of water molecules bound to the lanthanide ion (q) $[(1/T_1)_{IS} = P_m/(T_{1m} + \tau_m)]$, in which P_m is the mole fraction of the bound water nuclei. For example, we have reported a reversible calcium-activated MR agent with four *N*-acetic acid moieties in which the presence of micromolar Ca(II) exhibits an increase in relaxivity due to modulation of q (11, 12). Based on this molecular framework, we have prepared a Zn(II)-activated MR contrast agent with only two *N*-acetic acid binding groups, which selectively bind Zn(II) over Ca(II) and Mg(II). Similar to what happens with fluorescent Zn(II) sensors, the loss of acetic acid groups improves the selectivity for Zn(II) by greatly reducing the ability of Ca(II) to bind (13).

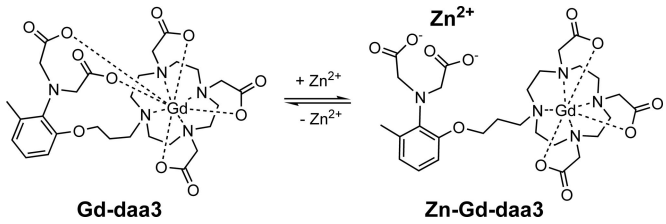

Fig. 1. Proposed mechanism of a Zn(II)-activated MR contrast agent whose observed signal proceeds from dark to bright in an acquired MR image. This increase in image intensity is a result of a selective change in the coordination environment of the complex upon binding of Zn(II).

The binding of Zn(II) to Gd-daa3 (daa3, diaminoacetate with three methylenes) is accompanied by a 114% increase in relaxivity at 60 MHz and 37°C due to a change in coordination geometry around the Gd(III) center (Fig. 1). Relaxivity and q measurements along with our nuclear magnetic relaxation dispersion (NMRD) data show that the increase in relaxivity is due to the coordination of one water molecule to Gd-daa3 in the presence of Zn(II). A second agent, Gd-daa2, with only two methylenes linking the gadolinium chelate with the zinc-binding aminoacetates, was synthesized and tested but showed little activation toward Zn(II).

Author contributions: J.L.M. and T.J.M. designed research; J.L.M. and G.P. performed research; J.L.M. contributed new reagents/analytical tools; J.L.M., G.P., and C.L. analyzed data; and J.L.M., G.P., C.L., and T.J.M. wrote the paper.

The authors declare no conflict of interest.

Abbreviations: daa3, diaminoacetate with three methylenes; DO3A, 1,4,7,10-tetraazacyclododecane-1,4,7-triacetic acid; DTPA, diethylenetriaminepentaacetate; MR, magnetic resonance; NMRD, nuclear magnetic relaxation dispersion; SBM, Solomon–Bloembergen–Morgan; ZFS, zero field splitting.

‖To whom correspondence should be addressed. E-mail: tmeade@northwestern.edu.

This article contains supporting information online at www.pnas.org/cgi/content/full/0706247104/DC1.

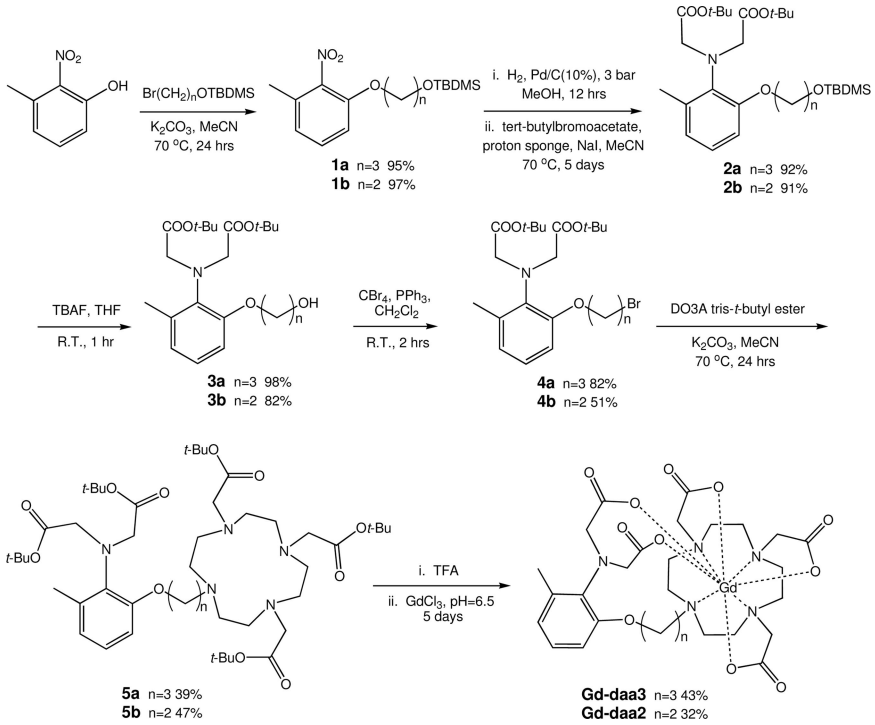

Fig. 2. Synthesis of Gd-daa3 and Gd-daa2. DO3A, 1,4,7,10-tetraazacyclododecane-1,4,7-triacetic acid; R.T., room temperature; TBAF, tetrabutylammonium fluoride; TBDMS, *t*-butyldimethylsilyl; TFA, trifluoroacetic acid.

MR contrast agents sensitive to Zn(II) concentration have been reported that are based on the binding of Zn(II) to *N*,*N*,*N*′,*N*′-tetrakis(2-pyridylmethyl)ethylenediamine (TPEN) (14, 15). However, these agents show a decrease in relaxivity upon binding of Zn(II) [and therefore, a bright-to-dark signal upon Zn(II) binding], whereas the complex reported here provides an increase in relaxivity upon Zn(II) binding (dark-to-bright image), which definitively reports the presence of zinc. A negative feedback probe can mean that there is zinc present, but the signal could be decreasing in brightness because of diffusion of the agent, thereby giving inconclusive results. An MRI agent similar to Gd-daa3 found to be activated by Cu(II) has been reported as well (16). While the authors of ref. 16 report a small response due to Zn(II) binding, their measurements were done in PBS, which would show little effect of zinc binding due to the immediate precipitation of $Zn_3(PO_4)_2$ (17). Our measurements done in a noncoordinating Hepes buffer give a more accurate account of the binding properties of this agent.

With a >100% increase in relaxivity, and a binding constant of 240 μM, our agent may have the ability to allow visualization of changes in Zn(II) concentrations in extracellular fluids of the brain. The release of high concentrations of Zn(II) (200–300 μM) from neuronal synaptic vessels into the extracellular fluids of the brain (≈10 nM) (18, 19) when under stress has been implicated in a variety of pathological functions, including the precipitation of β-amyloid plaques seen in Alzheimer's disease (18).

Results and Discussion

Gd-daa3 and Gd-daa2 were synthesized as shown in Fig. 2. The synthesis begins with alkylation of the commercially available 3-methyl-2-nitrophenol to yield the protected alcohol product **1**. The nitro group was reduced to the amine under standard palladium-catalyzed hydrogenation conditions and reacted immediately with *t*-butylbromoacetate under basic conditions. Product **2** was reacted with tetrabutylammonium fluoride to remove the TBDMS protecting group and then brominated to give compound **4**. DO3A tris-*t*-butyl ester was synthesized by following a literature procedure (20) and combined with **4** to prepare the fully *t*-butyl-protected ligand **5**. After removal of the *t*-butyl groups with trifluoroacetic acid, the ligand was dissolved in water and the pH was adjusted to 6.5 with 1 M NaOH. $GdCl_3$ was added to the ligand while maintaining a constant pH for a period of 5 days. Unreacted gadolinium was precipitated as $Gd(OH)_3$ with 1 M NaOH and separated by centrifugation. The final compounds were then purified by semipreparatory HPLC and characterized by LC-MS and elemental analysis [see supporting information (SI) *Materials and Methods*].

The relaxivities of Gd-daa3 and Gd-daa2 were measured at 60 MHz and 37°C in the absence and presence of $ZnCl_2$. In the absence of Zn(II) the relaxivity of Gd-daa3 in Hepes buffer is 2.3 $mM^{-1}{\cdot}s^{-1}$, consistent with a $q = 0$ complex (8). Addition of $ZnCl_2$ increases the relaxivity to 5.1 $mM^{-1}{\cdot}s^{-1}$. The overall difference in relaxivity [before and after addition of Zn(II)] is 73% and is sufficient for *in vivo* detection.** Similar studies were conducted with $MgCl_2$ and $CaCl_2$ to test the selectivity of Gd-daa3 for Zn(II) over other biologically abundant divalent cations known to have higher cellular concentrations and that have similar binding affinities toward carboxylic acid ligands. There is no significant change in relaxivity for either Mg(II) or Ca(II) even when an excess of these divalent cations was added (Fig. 3). Relaxivity measurements with $CuCl_2$ in Hepes buffer show an increase from 3.1 $mM^{-1}{\cdot}s^{-1}$ to 5.1 $mM^{-1}{\cdot}s^{-1}$ upon the addition of 1 eq of copper. Although Cu(II) binding is possible, its concentration is 1/10 that of Zn(II) during neurotransmission, where we would be most interested in imaging zinc (21). Estimates of Cu(II) concentration are only ≈30 μM, whereas Zn(II) is expected to be at least 300 μM (21).

**Gd diethylenetriaminepentaacetate (DTPA) has a relaxivity of 3.8 $mM^{-1}{\cdot}s^{-1}$ at 60 MHz and 310 K. In the absence of Zn(II), Gd-daa3 has a 40% lower relaxivity (2.3 $mM^{-1}{\cdot}s^{-1}$) than Gd-DTPA, and in the presence of Zn(II), it has 33% higher relaxivity (5.1 $mM^{-1}{\cdot}s^{-1}$) than Gd-DTPA.

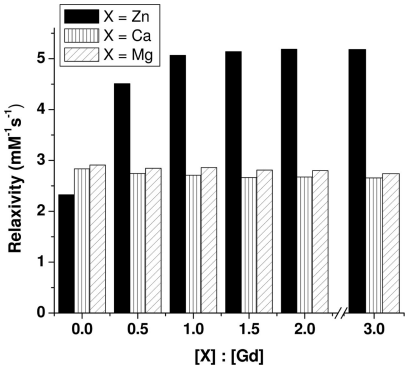

Fig. 3. Relaxivity of Gd-daa3 at 60 MHz and 310 K in the presence of XCl_2, where X = Zn(II), Ca(II), or Mg(II). All solutions were prepared in 100 mM KCl/100 mM Hepes at pH 7.4.

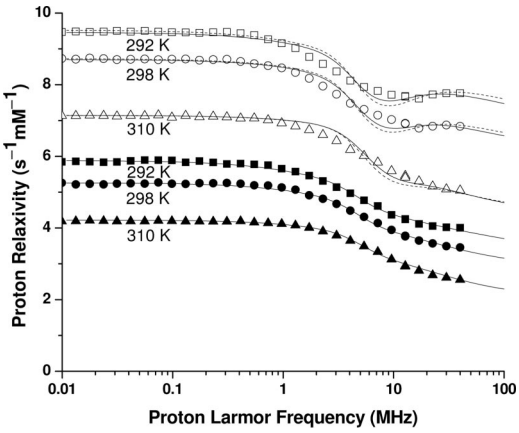

Fig. 4. Water proton relaxivity data for Gd-daa3 in the absence (filled symbols) and in the presence (open symbols) of Zn(II) at various temperatures (squares = 292 K, circles = 298 K, and triangles = 310 K). The solid and dashed lines are best-fit curves to approximate theories for (*i*) fast-rotating complexes in the absence of static zero field splitting (ZFS) or (*ii*) slow-rotating complexes in the presence of static ZFS, respectively.

To determine the efficiency of Gd-daa3 under physiological conditions, relaxivity measurements were done in male human blood serum. An overall increase in relaxivity was again observed as Zn(II) was added (see SI Fig. 7). The relaxivity increases from 5.8 $mM^{-1}{\cdot}s^{-1}$ to 7.7 $mM^{-1}{\cdot}s^{-1}$ in the presence of Zn(II) at 37°C and 60 MHz, providing a 33% increase in relaxivity, sufficient for visualization in MRI.

More interestingly, Gd-daa2 showed no change in relaxivity upon addition of $ZnCl_2$, suggesting that Gd-daa3 may have the optimal binding properties to both Gd(III) and Zn(II) for a Zn(II)-sensitive agent. The low relaxivity of Gd-daa2 in the absence of Zn(II), 1.44 $mM^{-1}{\cdot}s^{-1}$, suggests a complex that more efficiently blocks the access of water in its closed state, possibly due to tighter binding of the aminoacetate arms to Gd(III).

Values of q were determined by preparing the terbium analog (Tb-daa3) and acquiring time-based fluorescence microscopy measurements. The fluorescence decay rates of Tb-daa3 in water and D_2O can be related to q (22). The decay times in water were 1.46 ms and 1.96 ms with and without zinc, respectively, and 2.65 ms and 2.71 ms for D_2O. By using the equation for Tb ($q = 4.2$ ms $[(1/t_{H_2O}) - (1/t_{D_2O}) - 0.06]$) (22), q was calculated to be 0.3 ± 0.1 with no zinc present and 1.0 ± 0.1 in the presence of zinc. These numbers are consistent with our proposed mechanism depicted in Fig. 1 and introduced previously with our calcium-activated MR agent.

The NMRD profiles of Gd-daa3, measured in the presence and absence of Zn(II) at 292, 298, and 310 K, are reported in Fig. 4. The observed bulk water proton relaxivity is provided by the sum of (*i*) the outer-sphere contribution, due to the dipolar interaction between unpaired electrons and protons of freely diffusing water molecules, and (*ii*) the inner-sphere contribution. The latter is due to the dipolar interaction between unpaired electrons and protons of water molecules coordinated to the paramagnetic ion (first sphere) or anchored at a fixed distance r from the metal ion (second sphere) in exchange with bulk water protons. When such exchange is fast (i.e., the exchange rate is faster than the relaxation rate of the protons of bound water molecules), the observed bulk water proton relaxivity is a good reporter of the presence of water molecules coordinated to the metal ion. A slow exchange regime, on the other hand, is characterized by an increase in relaxivity with increasing temperature (12) as the exchange rate increases with temperature.

An overall increase in relaxivity is observed at all fields in the Zn(II)-containing sample. Such increase is in agreement with a larger hydration of the gadolinium site. The decrease in relaxivity with increasing temperature actually indicates the occurrence of a fast exchange regime for the inner-sphere relaxation. Outer-sphere relaxation is always expected to decrease with increasing temperature. One dispersion is present in all profiles, at ≈2–10 MHz, as expected for both the outer-sphere relaxation and the inner-sphere relaxation for complexes with reorientation times of the order of 100 ps, in agreement with the molecular weight of the present system, and electron relaxation times typical of gadolinium complexes (23, 24). The increase in relaxivity at high frequencies, observed for the profiles of the Zn(II)-containing sample acquired at the lower temperatures, indicates the field dependence of the electron relaxation time.

The analysis performed according to current theories (23) confirms that in the absence of Zn(II) the outer-sphere contribution is dominant, setting an upper limit for the possible fraction of coordinated water $q = 0.3 \pm 0.2$, calculated for water protons at a typical distance for the first coordination sphere of Gd(III) (≈3.1 Å). The relaxation rates can be very well reproduced by using the Freed model (25) and the Solomon–Bloembergen–Morgan (SBM) theory (26, 27) by the simultaneous contributions of outer-sphere relaxation and second-sphere relaxation (solid lines in Fig. 4). The second-sphere relaxation is due to the presence of two water protons at 3.7 Å from the metal ion with a field dependence for the electron relaxation rates similar to what is obtained for Gd-DTPA (23, 24).

The overall increase in the relaxation rate values obtained for the Zn(II)-coordinated complex (open symbols in Fig. 4) can be reproduced with SBM theory considering the presence of an additional regularly coordinated water molecule: $q = 1.2 \pm 0.3$ is in fact obtained (see SI Table 1). The best-fit profiles (solid lines in Fig. 4) are satisfactory although not always in perfect agreement with the experimental data, probably because of the presence of both static and transient ZFS, as expected for Gd(III) complexes. Presently, available fitting programs cannot properly account for their simultaneous presence in fast-rotating systems. The SBM theory in fact neglects the presence of static ZFS. Data were also analyzed by using a slow-rotation program including ZFS (28, 29). Even in such a model, the data are consistent with the presence of a regularly coordinated water molecule (dashed lines in Fig. 4) These results indicate that a water molecule in fast exchange is regularly coordinated to the Gd(III) ion in the presence of Zn(II), whereas it is not detected in the absence of Zn(II), in agreement with the scheme depicted in Fig. 1.

Proton relaxivity measurements on Gd-daa3 were also performed while titrating with increasing amounts of Zn(II) up to 1:1.4 (Gd:Zn) eq. The titration showed a linear increase in the

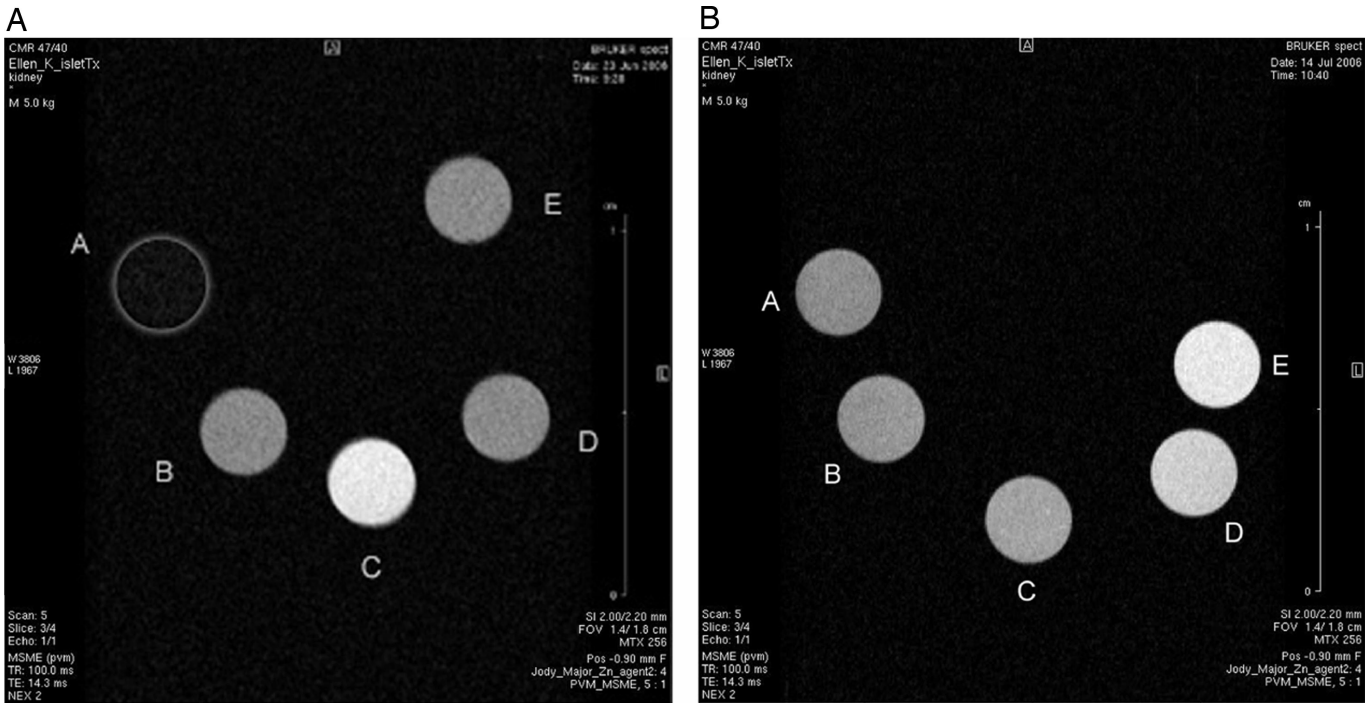

Fig. 5. T_1-weighted phantom MR images. (*A*) Gd-daa3 selectivity. Images of a 1 mM solution of Gd-daa3 in Hepes buffer. Spot A, Hepes buffer only; B, Gd-daa3; C, Gd-daa3 with 1 mM $ZnCl_2$; D, Gd-daa3 with 1 mM $MgCl_2$; and E, Gd-daa3 with 1 mM $CaCl_2$. (B) Gd-daa3 sensitivity. Images of a 1 mM solution of Gd-daa3 in Hepes buffer with various concentrations of $ZnCl_2$. Spot A, 0 μM Zn; B, 50 μM Zn; C, 100 μM Zn; D, 500 μM Zn; and E, 1 mM Zn. Repetition time (TR) = 100.0 ms; echo time (TE) = 14.3 ms; field of view (FOV) = 2.5/2.0 cm; data matrix = 256 × 256.

observed relaxation rate enhancement until 1:0.8 (Gd:Zn) eq, and then the rate leveled to a plateau at 1.2–1.4 eq. This observation confirms that a 1:1 (Gd:Zn) complex is formed, because relaxivity did not increase when Zn(II) was added in excess. The observed linear dependence also rules out the possibility of a 2:1 (Gd:Zn) complex formation.

To evaluate the effectiveness of Gd-daa3 as a potential *in vivo* probe the stability of Zn–Gd-daa3 was investigated. Using the commercially available fluorophore FluoZin-1 (Invitrogen, Carlsbad, CA), one can determine the binding constant of zinc by a competitive assay. Because the Zn(II)-binding regions of the dye and Gd-daa3 are identical, similar binding constants are to be expected. When the published dissociation constant for the dye (8.6×10^{-6} M) (13) was used, the K_d of Zn–Gd-daa3 was calculated to be 2.4×10^{-4} M. A primary goal of this research is to prepare a series of MR agents with a range of binding constants for Zn(II) for *in vitro* and *in vivo* studies, and Gd-daa3 is the first example. Gd-daa3 is sensitive enough to bind Zn(II) in the concentration range of $\approx$100 μM, allowing us to investigate MR imaging of Zn(II) release in the brain.

In vitro MR images on a 4.7-T magnet show an increase in intensity for Gd-daa3 in the presence of Zn(II), whereas there is no discernible difference of Gd-daa3 with Ca(II) or Mg(II) (Fig. 5*A*). More importantly, phantom images of various Zn(II) concentrations show that we can easily visualize the difference between 100 μM and 500 μM zinc (Fig. 5*B*). To confirm there was a measurable difference between zinc concentrations, T_1 was measured on these same samples on a 14.1-T magnet and on a 1.4-T magnet (data in SI Tables 2 and 3).

Gd-daa3 was monitored for 24 h in a 0.1 M phosphate buffer to determine its stability in solution. Because of the low solubility of $GdPO_4$ ($K_{sp} = 10^{-22.26}$ mol^2·liter^{-2}) (30) any dissociation of gadolinium from Gd-daa3 will precipitate, causing a subsequent decrease in relaxivity, which was not seen (17). A more accurate measurement of the amount of gadolinium dissociation can be made from centrifuging the samples and collecting aliquots of the supernatant for evaluation of gadolinium concentration by inductively coupled plasma mass spectrometry. This was done at various time points up to 24 h, and it was found that there was no significant change in [Gd], indicating no loss of gadolinium from the Gd-daa3 complex. This suggests a dissociation constant for Gd-daa3 on the order of that seen for Gd-DO3A (log K_d = 21) and its derivatives.

Treatment of NIH/3T3 cells with 0.5 mM Gd-daa3 for up to 24 h shows no observable cell death as visualized by trypan blue staining. Cells proliferated exponentially at the expected rate, indicating low toxicity from the agent (Fig. 6*A*). Gd-daa3 was effectively taken up by NIH/3T3 cells at a constant rate for the first 8 h of treatment. The maximal intracellular concentration of Gd-daa3 of $\approx 10^{-14}$ mol Gd/cell is achieved at 8 h and maintained up to 24 h (Fig. 6*B*). These results provide support for potential *in vivo* studies in the future.

In summary, we have presented the design and synthesis of a Zn(II)-activated MR contrast agent for which an increase in image intensity is observed upon exposure to physiologically relevant concentrations of Zn(II). Gd-daa3 shows high selectivity of Zn(II) over Ca(II) and Mg(II). Upon binding of Zn(II) the relaxivity is more than doubled. Relaxivity studies conducted in human blood serum prove the capability of translation into *in vivo* experiments. This is the first generation of Zn(II)-activated MR contrast agents with an increase in relaxivity, and we hope that investigating future generations will provide a range of zinc binding affinities. NMR investigation of solution structures should allow us to test the suggested mechanism of the change in coordination geometry about the Gd(III) ion in the presence of Zn(II).

Materials and Methods

General Methods. $GdCl_3·6H_2O$, $TbCl_3·6H_2O$, and 1,4,7,10-tetraazacyclododecane (cyclen) were purchased from Strem Chemicals (Newburyport, MA). FluoZin-1 was purchased from

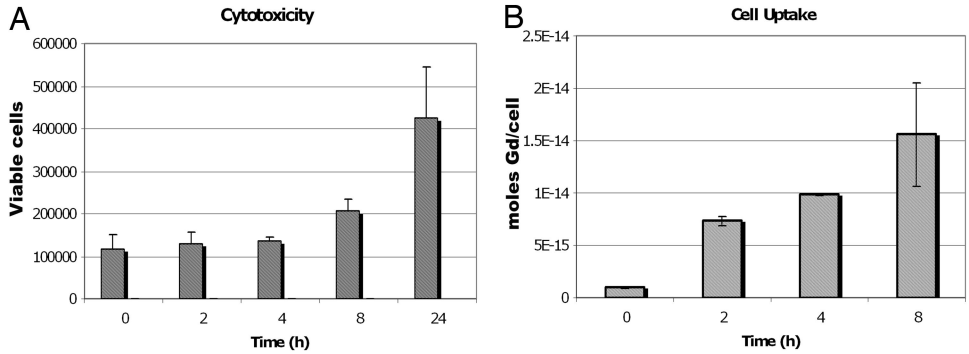

Fig. 6. Cell cytotoxicity and uptake of 0.5 M Gd-daa3 with NIH/3T3 cells. (*A*) Normal proliferation of NIH/3T3 cells is seen when they are incubated with 0.5 M Gd-daa3. The cell doubling time for NIH/3T3 cells is ≈16 h, and we can see over twice as many cells at 24 h than at 8 h as we would expect, implying >99% cell viability. (*B*) Gd-daa3 is taken up at a constant rate for up to 8 h.

Invitrogen. Male human blood serum was obtained from Sigma (St. Louis, MO) (catalog no. H 1388). All other chemicals were purchased and used as is from Sigma–Aldrich. NMR spectra were recorded on either Varian (Palo Alto, CA) Mercury 400-MHz or Varian Inova 500-MHz instruments with deuterated chloroform as the solvent. All spectra were referenced to an internal tetramethylsilane standard. Electrospray mass spectra were obtained on a Varian 1200L single-quadrupole mass spectrometer. All samples were prepared in a 100 mM KCl/100 mM Hepes buffer at a pH of 7.4 unless otherwise noted.

Relaxivity Measurements. The efficacy of these agents for use as MRI contrast agents is measured by their relaxivity value, the slope of the line of the reciprocal of T_1 versus the concentration of gadolinium. A 1 mM solution of the gadolinium complex was made up in buffer containing 100 mM KCl and 100 mM Hepes at pH 7.4 or in human blood serum. These were serially diluted four times to give 500 μl of five different sample concentrations at a [Gd]:[Zn] ratio of 1:0. $ZnCl_2$ was added to each of the samples to give a [Gd]:[Zn] ratio of 1:0.5. After 30 min of incubation at 37°C, T_1 measurements were made. This titration was repeated until a 1:3 ([Gd]:[Zn]) ratio was reached. Similar titration experiments were done with $CaCl_2$ and $MgCl_2$ to test the effects of competing cations. Results for Gd-daa3 are summarized in Fig. 3. The titrations were done in the same manner for Gd-daa2 up to a ratio of 1:2 ([Gd]:[X], where X = Zn, Mg, or Ca) (see SI Fig. 8). No significant changes in relaxivity were seen.

Luminescence Lifetime Measurements. The fluorescence decay rates of Tb-daa3 in H_2O and D_2O were measured on a Hitachi (San Francisco, CA) F4500 fluorimeter monitoring the emission at 544 nm with an excitation at 254 nm. A 200 μM solution of Tb-daa3 in Hepes buffer was measured in the presence of 300 μM $ZnCl_2$ and without $ZnCl_2$. Twenty-five scans were averaged and fit to a monoexponential decay with an r^2 value of 0.99.

NMRD. Longitudinal water proton relaxation rates were measured with a Stelar (Mede, Italy) Spinmaster FFC-2000-1T fast-field cycling relaxometer in the 0.01- to 40-MHz proton Larmor frequency range, using the standard field cycling protocol (31). R_1 values were obtained with an error smaller than 1%. Proton NMRD profiles were thus obtained by plotting proton relaxation rates as a function of applied magnetic field. The NMRD data, subtracted from the diamagnetic contribution of buffer alone and normalized to 1 mM Gd(III) concentration, were then analyzed in terms of inner-sphere and outer-sphere effects (23). Gd(III) complexes are expected to have both static and transient ZFS. Presently available fitting programs cannot properly account for their simultaneous presence in fast-rotating systems. Therefore, we analyzed the data by using either SBM theory (no static ZFS) or slow-rotation programs including ZFS (28, 29).

Calculation of Zn Binding Constant. A 10 μM sample of $ZnCl_2$ in Hepes buffer was titrated with 100-μl aliquots of 0.1 mM FluoZin-1 (Invitrogen) until saturation of fluorescence was reached. Between aliquots, 30 min was allowed for the reaction to reach equilibrium. Gd-daa3 at various concentrations in 10 μM $ZnCl_2$ was then titrated with FluoZin-1 in the same manner (see SI Fig. 9). Assuming a 1:1 (Gd:Zn) complex is formed, the following equilibrium is established in solution. After each aliquot of fluorophore was added, the percent saturation of fluorescence [$f = (F - F_0)/(F - F_{max})$, where F_0 is the minimum fluorescence without zinc and F_{max} is the fluorescence when saturated with zinc], was calculated to determine the amount of Zn(II) bound to the dye. With known amounts of Zn(II), FluoZin-1, and Gd-daa3, the equilibrium constant was determined.

$$\text{Zn–Gd-daa3} + \text{FluoZin} - 1 \rightleftharpoons \text{Zn-FluoZin} - 1 + \text{Gd} - \text{daa3}$$

$$K_{eq} = \frac{[\text{Zn-FluoZin-1}][\text{Gd-daa3}]}{[\text{Zn-Gd-daa3}][\text{FluoZin-1}]}$$

$$f = (F - F_0)/(F_{max} - F_0)$$

$$[\text{Zn} - \text{FluoZin} - 1] = f[\text{FluoZin} - 1]_T$$

$$[\text{FluoZin-1}] = [\text{FluoZin-1}]_T - [\text{Zn-FluoZin-1}]$$

$$[\text{Zn–Gd-daa3}] = [\text{Zn}]_T - [\text{Zn-FluoZin-1}]$$

$$[\text{Gd-daa3}] = [\text{Gd-daa3}]_T - [\text{Zn-Gd-daa3}].$$

MRI. *In vitro* phantom MR images were obtained of Gd-daa3 in Hepes buffer with 1 mM Zn(II), Mg(II), or Ca(II) ions loaded in 3-mm NMR tubes (Fig. 5*A*). Images were obtained on a 4.7-T horizontal-bore Bruker (Billerica, MA) Biospec using a multispin multiecho sequence. The phantom samples were prepared 1 h in advance of image acquisition. A second set of phantom images of 1 mM Gd-daa3 in Hepes buffer with Zn(II) concentrations of 0 μM, 50 μM, 100 μM, 500 μM, and 1 mM were imaged (Fig. 5*B*). The following parameters were used for both phantom sets: repetition time TR = 100.0 ms, echo time TE = 14.3 ms, field of view FOV = 2.5/2.0 cm, and data matrix = 256 × 256.

Cytotoxicity. NIH/3T3 cells were seeded at 10^5 cells per well in 24-well tissue culture plates with Dulbecco's modified Eagle's medium (DMEM) containing 10% bovine calf serum and

incubated overnight in a 5% CO_2 incubator at 37°C. The medium was then changed and Gd-daa3 was added at 500 μM. After 2, 4, 8, and 24 h, cells were washed three times with 1× PBS, exposed to 250 μl of 0.25% trypsin, and harvested. Cells were diluted with an equal volume of 0.4% trypan blue and counted on a hemocytometer. For measurement of cellular uptake of Gd-daa3, the treated cells were incubated with concentrated nitric acid at 70°C for 3 h. The dissolved cells were diluted into a 5-ml solution with 3% nitric acid and 5 parts per billion of an indium internal standard. The concentration of Gd(III) was then determined by using inductively coupled plasma mass spectrometry (ICP-MS).

We thank Ellen Kohlmeir for image acquisition and Allison Harney for cytotoxicity studies. This work was supported by the National Institutes of Health/National Institute of Biomedical Imaging and Bioengineering Grant 1 R01 EB005866-01 (to T.J.M.), National Cancer Institute Grant 5 U54 CA90810 (to T.J.M.), Department of Defense/Wayne State Subcontract 91008600 (to T.J.M.), and Ente CR Firenze (to C.L.). J.L.M. is a Scholar of the Chicago Chapter of the ARCS (Achievement Rewards for College Scientists) Foundation.

1. Stefanidou M, Maravelias C, Dona A, Spiliopoulou C (2006) *Arch Toxicol* 80:1–9.
2. Frederickson CJ, Koh J-Y, Bush AI (2005) *Nat Rev Neurosci* 6:449–462.
3. Takeda A (2000) *Brain Res Brain Res Rev* 34:137–148.
4. Vallee BL, Falchuk KH (1993) *Physiol Rev* 73:79–118.
5. Kikuchi K, Komatsu K, Nagano T (2004) *Curr Opin Chem Biol* 8:182–191.
6. Jiang P, Guo Z (2004) *Coord Chem Rev* 248:205–229.
7. Merbach A, Toth E (2001) *The Chemistry of Contrast Agents in Medical Magnetic Resonance Imaging* (Wiley, New York).
8. Caravan P, Ellison JJ, McMurry TJ, Laufer RB (1999) *Chem Rev* 99:2293–2352.
9. Moats RA, Fraser SE, Meade TJ (1997) *Angew Chem Int Ed Engl* **36,** 726–728.
10. Louie AY, Huber MM, Ahrens ET, Rothbacher U, Moats R, Jacobs RE, Fraser SE, Meade TJ (2000) *Nat Biotechnol* 18:321–325.
11. Li W-H, Fraser SE, Meade TJ (1999) *J Am Chem Soc* 121:1413–1414.
12. Li W-H, Parigi G, Fragai M, Luchinat C, Meade TJ (2002) *Inorg Chem* 41:4018–4024.
13. Gee KR, Zhou Z-L, Ton-That D, Sensi SL, Weiss JH (2002) *Cell Calcium* 31:245–251.
14. Hanaoka K, Kikuchi K, Urano Y, Nagano T (2001) *J Chem Soc Perkin Trans 2*, 1840–1843.
15. Hanaoka K, Kikuchi K, Urano Y, Narazaki M, Yokawa T, Sakamoto S, Yamaguchi K, Nagano T (2002) *Chem Biol* 9:1027–1032.
16. Que EL, Chang CJ (2006) *J Am Chem Soc* 128:15942–15943.
17. Laurent S, Vander Elst L, Copoix F, Muller RN (2001) *Invest Radiol* 36:115–122.
18. Frederickson CJ, Cuajungco MP, Frederickson CJ (2005) *J Alzheimers Dis* 8:155–160.
19. Budde T, Minta A, White JA, Kay AR (1997) *Neuroscience* 79:347–358.
20. Dadabhoy A, Faulkner S, Sammes PG (2002) *J Chem Soc Perkin Trans 2*, 348–357.
21. Barnham KJ, Masters CL, Bush AI (2004) *Nat Rev Drug Discov* 3:205–214.
22. Quici S, Cavazzini M, Marzanni G, Accorsi G, Armaroli N, Ventura B, Barigelletti F (2005) *Inorg Chem* 44:529–537.
23. Bertini I, Luchinat C, Parigi G (2005) in *^{1}H NMRD Relaxation in Solution of Paramagnetic Complexes and Metalloproteins*, Advances in Inorganic Chemistry Including Bioinorganic Studies, eds van Eldik R, Bertini I (Elsevier, San Diego), Vol 57, pp 105–172.
24. Powell DH, Dhubhghaill OMN, Pubanz D, Helm L, Lebedev YS, Schlaepfer W, Merbach AE (1996) *J Am Chem Soc* 118:9333–9346.
25. Hwang LP, Freed JH (1975) *J Chem Phys* 63:4017–4025.
26. Solomon I (1955) *Phys Rev* 99:559–565.
27. Bloembergen N, Morgan LO (1961) *J Chem Phys* 34:842–850.
28. Bertini I, Kowalewsi J, Luchinat C, Nilsson T, Parigi G (1999) *J Chem Phys* 111:5795–5807.
29. Kruk D, Nilsson T, Kowalewsi J (2001) *Phys Chem Chem Phys* 3:4907–4917.
30. Tweedle MF, Hagan JJ, Kumar K, Mantha S, Chang CA (1991) *Magn Reson Imaging* 9:409–415.
31. Bertini I, Luchinat C, Parigi G (2001) *Solution NMR of Paramagnetic Molecules: Applications to Metallobiomolecules and Models* (Elsevier, Amsterdam).